Available online at www.sciencedirect.com

jmr&t Journal of Materials Research and Technology

journal homepage: www.elsevier.com/locate/jmrt

Original Article

Substitutive effect of nano-SiO_2 for silica fume in ultra-high-performance concrete on fiber pull-out behavior

Taekgeun Oh [a], *Booki Chun* [a], *Seung Kyun Lee* [a], *Wonkyo Lee* [a], *Nemkumar Banthia* [b], *Doo-Yeol Yoo* [a,*]

[a] *Department of Architectural Engineering, Hanyang University, 222 Wangsimni-ro, Seongdong-gu, Seoul, 04763, Republic of Korea*

[b] *Department of Civil Engineering, The University of British Columbia, 6250 Applied Science Lane, Vancouver, BC, V6T 1Z4, Canada*

ARTICLE INFO

Article history:
Received 22 May 2022
Accepted 3 August 2022
Available online 12 August 2022

Keywords:
Ultra-high-performance concrete
Nano-SiO_2
Compressive strength
Autogenous shrinkage behavior
Single fiber pullout behavior

ABSTRACT

This study investigated the effect of substituting nano-SiO_2 for silica fume on the fiber-matrix interfacial bond performance of ultra-high-performance concrete (UHPC). In this study, silica fume was substituted by nano-SiO_2 in the weight range of 0–50%. The degree of pozzolanic reaction of binder materials was evaluated using the thermogravimetric analysis (TGA) and compressive strength measurement. The single fiber pull-out test was conducted along with a measurement of autogenous shrinkage to evaluate the interfacial bond. The degree of pozzolanic reaction of nano-SiO_2 was found to be higher than that of other binder materials. Although the packing density was predicted to increase continuously up to a substitution ratio of 50%, the highest compressive strength was obtained when 10% of silica fume was replaced by nano-SiO_2, which improved the compressive strength by 5.9% compared to that of the plain sample. The autogenous shrinkage increased with an increasing content of nano-SiO_2 up to 30%; however, it remained similar beyond the nano-SiO_2 content of 30%. The best pull-out performance was obtained when 20% of silica fume was replaced by nano-SiO_2, in which the average bond strength and pull-out energy were improved by approximately 21 and 68%, respectively. Therefore, substitution of 10–20% of silica fume by nano-SiO_2 was recommended as an optimal amount considering the improvements of the compressive strength and fiber-matrix bond performance of UHPC.

© 2022 The Author(s). Published by Elsevier B.V. This is an open access article under the CC BY license (http://creativecommons.org/licenses/by/4.0/).

1. Introduction

In the mid-1990s, ultra-high-performance concrete (UHPC) was introduced by Richard and Cheyrezy [1]. They developed a UHPC based on an optimization of mix proportion considering the packing density theory and inclusion of a high-volume content of steel fibers to overcome the drawbacks of ordinary concrete, such as low strength-to-weight ratio, low ductility, and low durability. Since then, UHPC has been

* Corresponding author.
E-mail address: dyyoo@hanyang.ac.kr (D.-Y. Yoo).

https://doi.org/10.1016/j.jmrt.2022.08.013

2238-7854/© 2022 The Author(s). Published by Elsevier B.V. This is an open access article under the CC BY license (http://creativecommons.org/licenses/by/4.0/).

developed in many countries [2–5]. In general, UHPC is made of ordinary Portland cement, silica fume, silica flour, and a high-range water-redecreeing agent [6]. Silica fume is most widely used as a pozzolanic material for UHPC as it can improve the packing density owing to the filling effect and produce additional calcium silicate hydrate (C–S–H) gels owing to the pozzolanic reaction [1,7]. Thus, many studies have used various ranges of silica fume in UHPC, where the optimal amount of silica fume has been suggested to be in the range of 20–30% [1,8,9]. According to the existing studies, the optimum amount of silica flour as a filler is in the range of 30–40% of the weight of cement, whereas that of silica sand is 110% of the weight of cement [6,8].

In recent years, various types of nanomaterials have been introduced into UHPC to further improve its performance. Long et al. [10] reported that the addition of a small amount of nanomaterials remarkably affects the mechanical strength, degree of hydration, and pore structure of UHPC. Shi et al. [11] similarly explained that although nanomaterials have a high embodied carbon dioxide (CO_2), adding small amounts of nanomaterials is effective, even in the case of eco-friendly UHPC mixtures. The nanomaterials available for UHPC can be classified into two categories: inert nanomaterials with no reactivity and active nanomaterials with reactivity. Inert nanomaterials, such as graphene oxide, carbon nanofibers, carbon nanotubes, and nano-TiO_2, improve the material properties of cementitious composites mainly through filler, nucleation, and bridging effects. The reactive nanomaterials are generally more effective because they affect the hydration process of cement matrix using the pozzolanic reaction together with the filler and nucleation effects. Thus, many studies [12–19] have attempted to further improve the material performance of UHPC using these reactive nanomaterials.

Camiletti et al. [12] and Wu et al. [13] adopted nano-calcium carbonate ($CaCO_3$) in UHPC and reported that well-crystalline nano-$CaCO_3$ particles provide seeds for the nucleation reaction sites of C–S–H gels, leading to an accelerated hydration reaction of cement. The addition of an appropriate amount of nano-$CaCO_3$ improved the mechanical properties, such as the bond strength, compressive strength, and flexural strength; however, beyond a nano-$CaCO_3$ content of 3.2%, the mechanical properties decreased owing to an increase in porosity because of the agglomeration of nano-$CaCO_3$ [13]. Norhasri et al. [14] and Habeeb et al. [15] reported that the mechanical properties were improved by the pozzolanic reaction through the addition of nanometakaolin. Yu et al. [18] studied the effect of nano-silica (SiO_2) on the hydration and microstructure of UHPC with a low binder; optimal mechanical properties were found when the nano-SiO_2 content was 3.74%. Kontolenotos et al. [19] investigated the physicomechanical properties and microstructure of ultrafine cement with colloidal nano-SiO_2 and reported that although the effect of incorporating nano-SiO_2 was not immediately obtained at an early age, the highest compressive strength was obtained when the nano-SiO_2 content was 4%.

Similarly, many studies [12–19] have been conducted on the utilization of active nanomaterials in UHPC to enhance its mechanical properties. The use of nano-SiO_2 is considered an effective method because of its high pozzolanic reactivity and chemical composition similar to that of silica fume, which is a fundamental ingredient of ordinary UHPC. However, most of the previous studies used small amounts of nano-SiO_2 in the range of approximately 3–4% by weight of cement to replace ordinary Portland cement. This study aims to evaluate the mechanical strength and fiber-matrix interfacial bond performance of UHPC by substituting large amounts of nano-SiO_2 for silica fume, which has a similar chemical composition to nano-SiO_2.

2. Materials and method

2.1. Measurement of packing density

The packing density theory is typically used in the mix design of UHPC because it comprises various ingredients with other particle sizes, shapes, etc. Therefore, to investigate the effect of substitution ratio of nano-SiO_2, a compressible packing model was adopted [20]. Prior to the virtual packing density calculation, the particle size and wet packing density of each component were measured. The wet packing density was measured as follows: First, half of the ingredients and water were mixed with a polycarboxylate-based superplasticizer (SP). Second, the remaining ingredients were divided into four parts, and each ingredient was placed individually in a bowl. Third, all mixing procedures were conducted at a low speed for 3 min, and then the ingredient suspension was filled in a 30-ml cylinder mold. Subsequently, the fully filled mold was weighed. Finally, the virtual packing density (γ_i) was calculated as follows:

$$\gamma_i = \frac{\beta_i}{1 - \sum_{j=1}^{i-1} y_j \left[1 - \beta_i + \beta_i b_{ji}\left(1 - \frac{1}{\beta_j}\right)\right] - \sum_{j=i+1}^{n} y_j \left(1 - a_{ij}\frac{\beta_i}{\beta_j}\right)} \quad (1)$$

where β_i and β_j are the residual packing densities of the granular classes i and j, respectively, and y_j is the volume fraction of class j. a_{ij} and b_{ji} are the coefficients related to the interaction of each particle, which are called loosening and wall effects, respectively.

If the fine particles fill the voids between the coarse particles and can no longer fill the voids, that is, when the coarse particles are dominant, a loosening effect is generated. In contrast, when the coarse particles are surrounded by fine particles to form a wall-like boundary, that is, when the fine particles are dominant, a wall effect is generated. De Larrard [20] summarized the loosening and wall effects in simple equations, respectively, as follows:

$$a_{ij} = \sqrt{1 - \left(1 - \frac{d_j}{d_i}\right)^{1.02}}, \quad (2)$$

$$b_{ji} = 1 - \left(1 - \frac{d_i}{d_j}\right)^{1.5}, \quad (3)$$

where d_i and d_j are the mean particle sizes of different ingredients.

The virtual packing density γ of the granular mix is expressed as follows [20]:

$$\gamma = \min_{1 \le i \le n} \gamma_i \tag{4}$$

The actual packing density Φ can be calculated by considering the compaction index K and virtual packing density γ_i. The compaction index and packing density are defined as follows:

$$K = \sum_{i=1}^{n} K_i = \sum_{i=1}^{n} \frac{y_i / \beta_i}{1/\Phi - 1/\gamma_i}, \tag{5}$$

$$K = H\left(\frac{\Phi_i}{\Phi_i^*}\right), \tag{6}$$

where y_i is the volume fraction of class i, Φ_i is the actual solid volume of class i, Φ_i^* is the maximum volume that particle i may occupy when other particles exist.

2.2. Properties of ingredients and mixing process

Ordinary Portland cement (OPC), silica fume, silica flour, and silica sand were used to fabricate an ordinary UHPC mixture. OPC and silica fume were used as the binders, where silica flour and silica sand were used as the filler and aggregate, respectively. The scanning electron microscopy (SEM), transmission electron microscopy, and particle size distribution of all ingredients are shown in Figs. 1 and 2. The very fine particles such as SF and nano-SiO2 are quite easy to agglomerate. To provide accurately the particle size distribution, ultrasonic treatment was conducted for 30 min before particle size distribution. The median particle sizes of OPC, SF, silica flour, and silica sand were found to be 11.45, 0.295, 4.75, and 236.2 μm, respectively. In this study, nano-SiO_2 produced by Ditto Technology was used. The median particle size of nano-SiO_2 was in the range of 100–150 nm.

OPC and silica flour have highly crystalline structures, whereas silica fume and nano-SiO_2 have mostly amorphous phases. Lau et al. [21] reported that amorphous phases exhibit a higher reactivity than crystalline phases. Because nano-SiO_2 exhibits a similar XRD pattern to that of silica fume, silica fume was substituted by nano-SiO_2 with a replacement ratio in the range of 0–50% at intervals of 10%. Their chemical

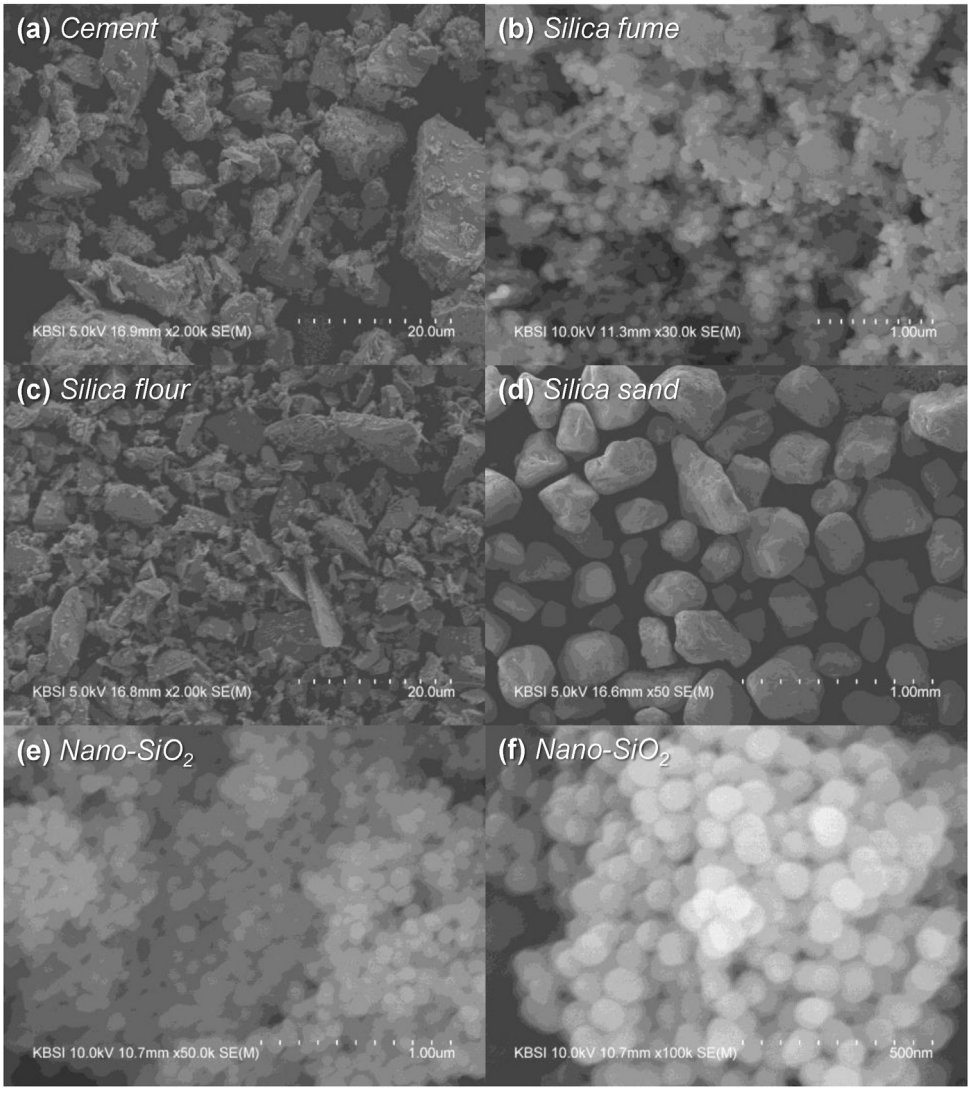

Fig. 1 – SEM image of all dry ingredients: (a) cement; (b) silica fume; (c) silica flour; (d) silica sand; (e) nano-SiO_2 at 50 k; (f) nano-SiO_2 at 100 k.

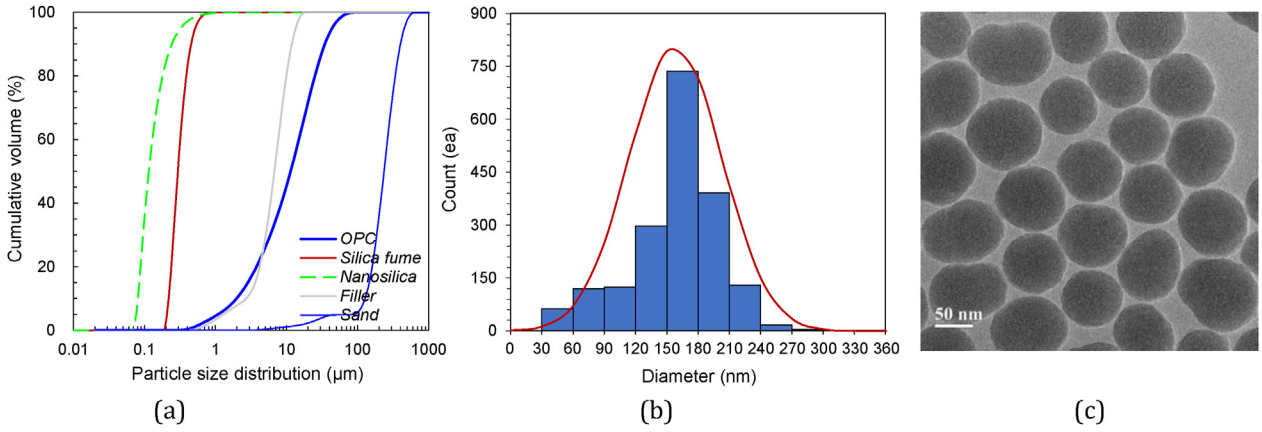

Fig. 2 – (a) Particle size distribution; (b) distribution histogram of nano-SiO_2 particles; (c) TEM image of nano-SiO_2.

compositions, physical properties, and mix proportions are listed in Tables 1 and 2, respectively. In this study, a large amount of nano-SiO_2 was added, which may cause an increase in material costs. However, due to the recent development of manufacturing technology [22], high-quality nano-SiO_2 can be synthesized at a low cost as well.

To satisfy the strength requirement of 150 MPa, as mentioned in ACI 239 [3], an extremely low water-to-binder ratio of 0.2 was adopted. A polycarboxylate-based SP composed of 30% solid and 70% water was used to achieve a self-consolidating property. All ingredients containing nano-SiO_2 were initially mixed using a Hobart-type mixer for 10 min. Water containing SP was then added to the mixed ingredients and mixed for 10 min. When the mixture satisfied a flow of 190 ± 10 mm, the fiber was incorporated into the mixture. The mixture containing the fiber was mixed for 5 min, and then fresh UHPC was cast in the prepared mold. The UHPC hardened after 48 h, and the specimens were cured in a water tank at a temperature of 90 °C for 3 d.

2.3. *Flow table test*

A flow table test was conducted to measure the flowability of a fresh UHPC. The standard test method for UHPC is prescribed in ASTM C1856 [23]; however, in this study, ASTM C1437 [24] was adopted to evaluate the effect of substituting silica fume by nano-SiO_2 in UHPC. The mold for the flow table test, with upper and lower diameters of 70 and 100 mm, respectively, was filled with a fresh UHPC mixture. The table was then immediately dropped 25 times in 15 s.

2.4. *Single fiber pull-out test*

Single-fiber pull-out test specimens were fabricated using the UHPC matrix, with the exception of the fibers. A thin PVC film with a cross-sectional area of 25 mm × 25 mm was placed at the center of the mold, and a single fiber was affixed to the PVC film. The inclination angle of the fiber was set in 0 and 45°. The target embedded length of the fiber was set to 8 mm to achieve only the pull-out failure mode and avoid fiber rupture. When the fiber was fixed in the mold, one side was cast with fresh UHPC matrix and cured for 48 h; the other side was filled and cured for 48 h. After demolding, the pull-out test samples were immersed in a water tank at a temperature of 90 °C for 3 d. The dog-born sample was affixed to the steel grips, and a uniaxial pull-out load was applied at a pull-out rate of 0.0018 mm/s. The pull-out load was measured to load the cell with a 3-kN capacity affixed universal testing machine (UTM), and the fiber slip from the matrix was measured from the displacement of the crosshead. The detailed test procedure is illustrated in Fig. 3.

2.5. *Compressive test*

Three test specimens with dimensions of 50 mm × 50 mm × 50 mm were produced to investigate the effect of

Table 1 – Chemical compositions and physical properties of dry ingredients.

Composition [%]	PC	Silica fume	Nano-SiO_2	Silica flour	Silica sand
SiO_2	18.8	92.6	99.9	97.0	97.2
Al_2O_3	4.18	0.07	–	0.45	0.05
Fe_2O_3	3.72	0.49	–	0.1	0.13
CaO	65.3	0.67	–	0.07	0.13
MgO	2.43	1.8	–	0.01	0.01
SO_3	3.28	0.12	–	–	–
Na_2O	0.15	0.02	–	–	–
K_2O	1.1	1.13	–	–	0.02
Specific surface area (cm^2/g)	3413	200,000	310,858	2232	–
Density	3.15	2.2	1.67	2.62	2.65

[Note] PC = Type I ordinary Portland cement.

Table 2 – Mix proportion of UHPC.

	W/B**	Mix design [kg/m^3]						
		Water	Cement	SF	Silica sand	Silica flour	Nano-SiO_2	SP*
NS0 (plain)	0.18	160.3	788.5	197.1	867.4	236.6	–	25.0
NS10	0.18			177.4			19.7	27.5
NS20	0.19			157.7			39.4	31.0
NS30	0.19			138.0			59.1	32.0
NS40	0.19			118.3			78.8	36.0
NS50	0.19			98.6			98.6	38.0

[Note] W/B = water-binder ratio and SP = superplasticizer.
*SP includes 30% solid and 70% water.
**W/B is calculated by considering the amount of water from SP.

nano-SiO_2 addition on the performance of the UHPC. Compressive tests were conducted according to ASTM C109 [25]. A compressive load was applied at a loading rate of 500 N/s, and the applied load was measured at the load cell attached to a UTM with a capacity of 200 t. The compressive strength was calculated by dividing the maximum load by a contact area of 50 mm × 50 mm.

2.6. *Autogenous shrinkage test*

To investigate the effect of nano-SiO_2 substitution for silica fume on the autogenous shrinkage of UHPC, prismatic molds with a cross-sectional area of 50 mm × 50 mm and length of 250 mm were prepared. A Teflon sheet was then attached to the molds to eliminate friction. According to Aïtcin [26], because the autogenous shrinkage of high-performance concrete causes a precipitous increase at an early age, it must be measured at the time of casting or before the fresh mixture hardens. Therefore, autogenous shrinkage of the UHPC matrix was measured before casting the fresh mixture. For UHPC without coarse aggregate and steel fiber, it is difficult to properly locate an embedded strain gauge and thermocouple; they were located in the center of the mold using a nylon line before the mixture was cast. After casting the fresh UHPC, the plastic sheet was immediately attached, to prevent water evaporation, and cured at 23 °C for 2 d. Subsequently, the specimen was demolded, and aluminum tape was attached, to prevent the evaporation of internal moisture, and cured for 26 d at the same temperature. The temperature and shrinkage strain were recorded using a data logger at intervals of 30 s

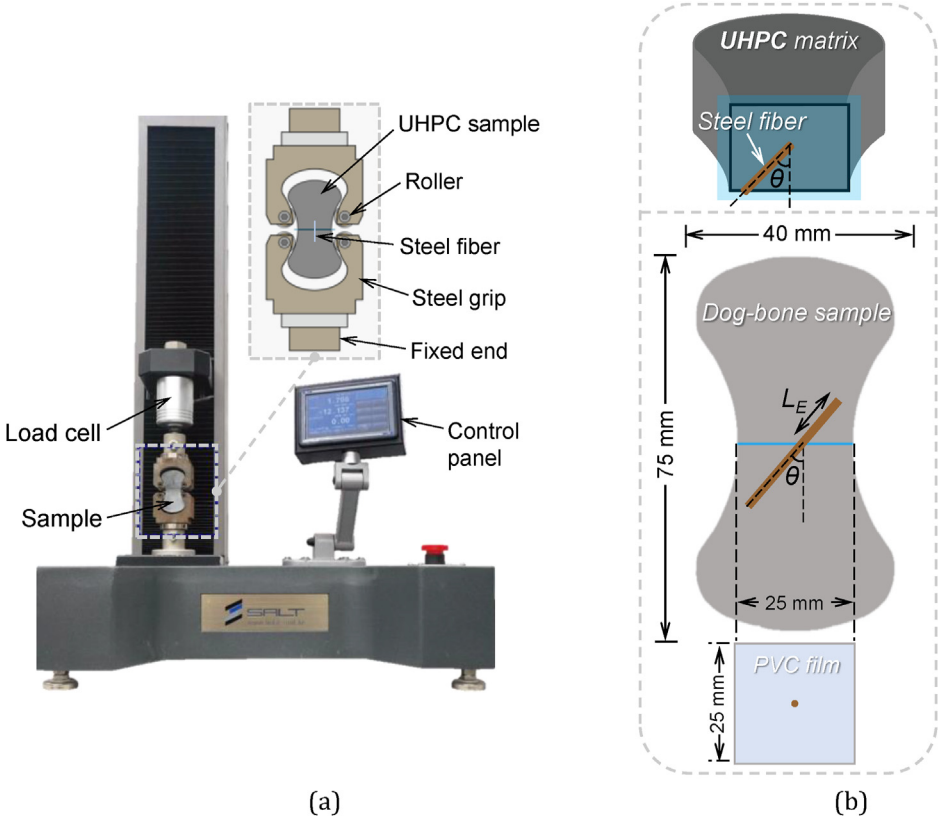

Fig. 3 – (a) Single fiber pullout test setup and (b) geometrical details of dog-bone sample.

and 5 min before and after the specimen was demolded, respectively. The detailed test setup is illustrated in Fig. 4.

3. Test results and discussion

3.1. Reactivity of nano-SiO_2 and silica fume to calcium hydroxide

To verify the pozzolanic reactivity of the binder materials, they were mixed with a calcium hydroxide (CH) solution. As a control sample, silica flour, which was used as a filler, was mixed with the CH solution, which was fabricated with CH:water = 1:10 by weight ratio. These different binders and filler materials were mixed with the same content of CH, and all samples were cured for 28 d in a desiccator with injected nitrogen gas to avoid the oxidation of CH during the curing period.

Fig. 5 depicts the thermogravimetry (TG) and derivative thermogravimetry (DTG) results activated with the CH solution after 28 days of curing. All binder materials, such as OPC, silica fume, and nano-SiO_2, exhibited obvious peaks at temperatures below 200 °C. These peaks indicate hydration products, that is, C–S–H gel, ettringite, and AFm phases, which were produced by the hydration or pozzolanic reaction with CH [27–29]. In particular, nano-SiO_2 had the highest peak because the diameter of nano-SiO_2 was very fine and the specific surface area was extremely large, leading to the highest reactivity. In the case of silica fume, the peak intensity was lower than that of the nano-SiO_2 sample, which is consistent with the findings of Ghafari et al. [30]. They reported that nano-SiO_2 has a higher reactivity than that of silica fume owing to its large specific surface area. This resulted in an improvement in the pozzolanic reaction at an early age. OPC exhibited a weak intensity, which may be owing to its chemical composition, which has an extremely low SiO_2 content of approximately 18.8%. Moreover, silica flour (filler) showed no DTG peaks below 200 °C. Thus, silica flour is inert and nonreactive, as reported by You et al. [31] and Oh et al. [32]. A CH-related DTG peak at approximately 400 °C was clearly detected in silica flour and OPC. In the case of OPC, because OPC also produced CH during the hydration reaction, the CH intensity increased [33]. In contrast, for silica fume and nano-SiO_2, no DTG peaks near a temperature of 400 °C was detected owing to exhaustion of all CH during the pozzolanic reaction. All samples had a DTG peak related to calcium carbonate at a temperature in the range of approximately 600–700 °C. The DTG results reveal that the degree of the pozzolanic reaction was high in the order of nano-SiO_2 > silica fume > OPC >> flour.

3.2. Flowability of nano-SiO_2 substituted UHPC

The results of the flow table test are shown in Fig. 6. The flow values of all samples were measured at 190 ± 10 mm because SP was additionally incorporated into the UHPC depending on the amount of nano-SiO_2. Fig. 6(b) shows an increase in SP with respect to the nano-SiO_2 content. The amount of SP to maintain a certain flow value of 190 mm was increased with an increasing nano-SiO_2 content in the fresh mixture. Meng and Khayat [34] reported that the addition of a small amount of nanomaterials can reduce the demand for a high-range water reducer (HRWR) by the lubrication effect; however, when a large amount of nanomaterials was added, HRWR increased again owing to the negative effects, that is, the adsorption effect of nanomaterials. Therefore, in this study, the SP demand was only increased because the content limitation of nano-SiO_2, which dominates the lubrication effect, was exceeded.

In addition, the increasing amount of nano-SiO_2 and SP affected the rate of hydration reactions. When a small amount of nano-SiO_2 was added, the hydration rate was accelerated by the pozzolanic reaction and nucleation effect of C–S–H. However, an increasing content of nano-SiO_2 is accompanied by an increase in the SP demand, which results in a delay in the hydration of the fresh mixture. The rate of the hydration reaction according to the nano-SiO_2 content is discussed in Subsection 3.4.2.

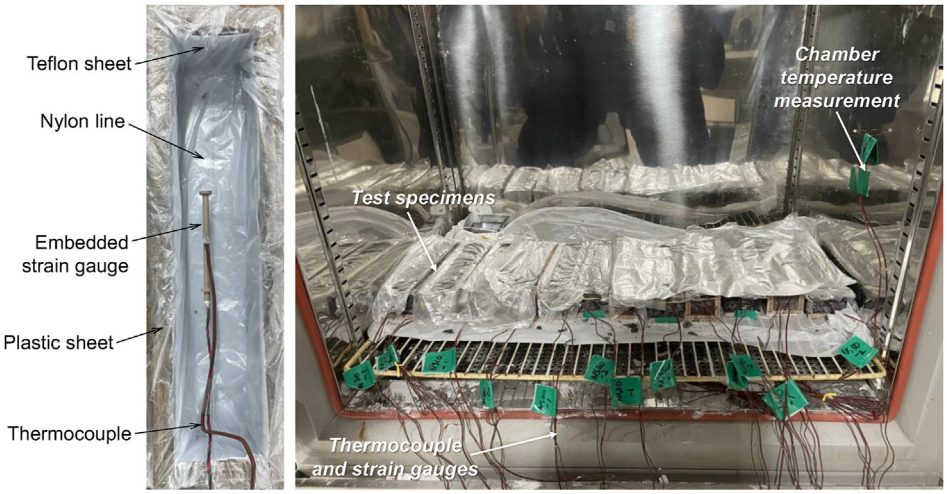

Fig. 4 – Test setup for autogenous shrinkage measurement.

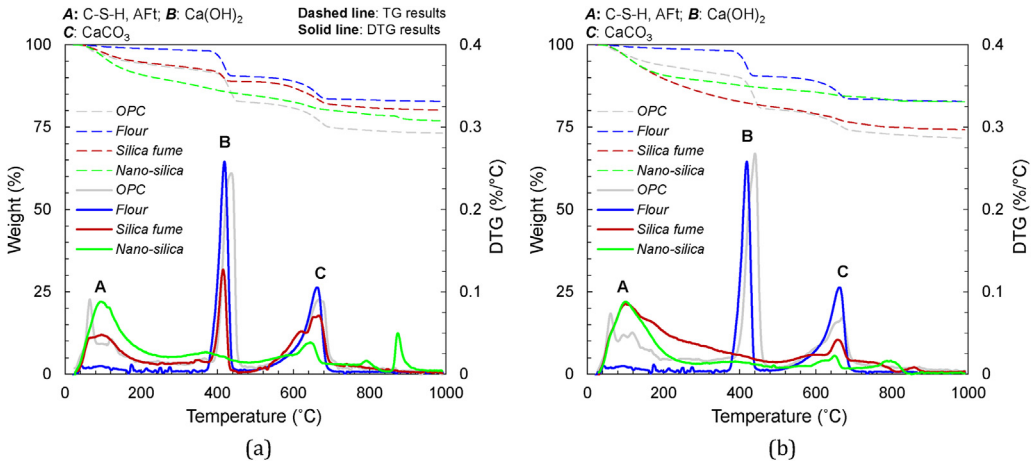

Fig. 5 – TG/DTG results after reacting binder materials and filler with CH solution at (a) 7 days and (b) 28 days.

3.3. *Effect of substitution ratio of nano-SiO_2 on the packing density and compressive strength*

Fig. 7 summarizes the virtual packing density and compressive strength of the UHPC matrices with various content of nano-SiO_2. The virtual packing density of UHPC without nano-SiO_2 was approximately 0.82, similar to that reported by Soliman et al. [35]. With an increasing substitution ratio, the packing density increased to 0.825 at a substitution ratio of 50%. Since the packing density of the NS0 specimen used as reference data was already optimized and very high because 20% of OPC was replaced with SF by weight ratio [36], the difference between the packing densities of NS0 and NS50 specimens was small. These results are not consistent with those of the compressive strength. The maximum compressive strength was obtained when silica fume was replaced with 10% nano-SiO_2, which was approximately 161.5 MPa and improved by approximately 5.9%. The improved compressive strength of UHPC at a substitution ratio of 10%, which is the optimal amount, was caused by the filler and nucleation effects [37]. The nano-SiO_2 particles can fill the voids of the C–S–H gel structure and act as nuclei to tightly bond with C–S–H gels, resulting in a denser matrix [37]. When the substitution ratio was increased, the compressive strength gradually decreased; however, the compressive strength was still higher than that of the plain UHPC (NS0). This phenomenon is associated with the combined effects of the agglomeration of very fine nano-SiO_2 and higher pozzolanic reactivity. In general, because very finer particles have high van der Waals and electrostatic forces, dispersion and mechanical strength decrease. However, the high reactivity of nano-SiO_2 improves the compressive strength by creating denser microstructures. Therefore, a higher compressive strength of NS50 than that of NS0 can be maintained.

3.4. *Autogenous shrinkage*

3.4.1. *Determination of the time zeroing point*

Fig. 8 shows the typical shrinkage strain and internal temperature–time curve of plain UHPC at the initial stage. When the fresh mixture was cast into a mold, the temperature and shrinkage strain of the specimen behaved comparably. In this study, the temperature of the fresh UHPC mixture was lower than the chamber temperature (23 °C), and the internal temperature and measured strain decreased immediately after casting. As the internal temperature converged to the

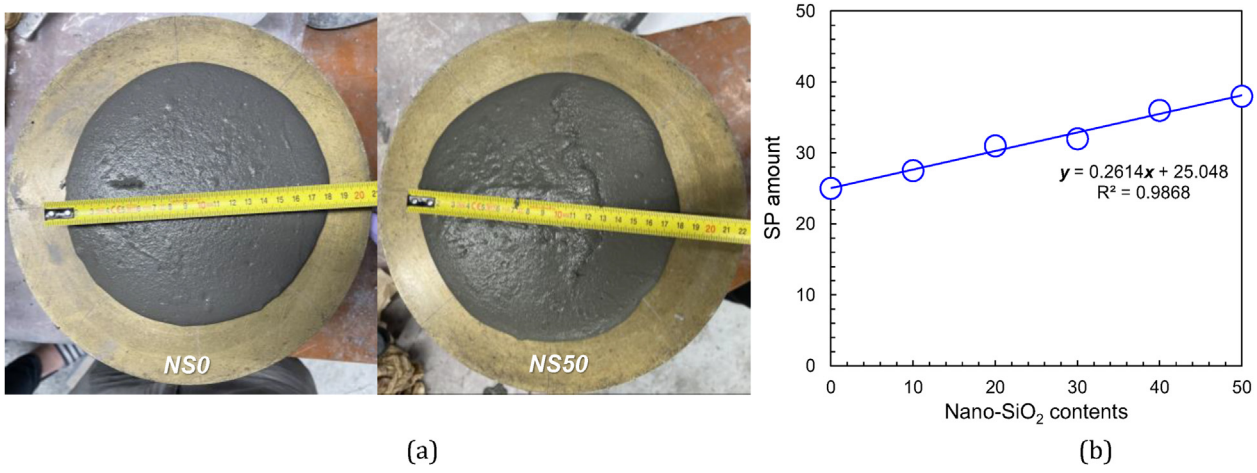

Fig. 6 – (a) Flow table test results of fresh UHPC with/without nano-SiO_2 and (b) SP demand with nano-SiO_2 contents.

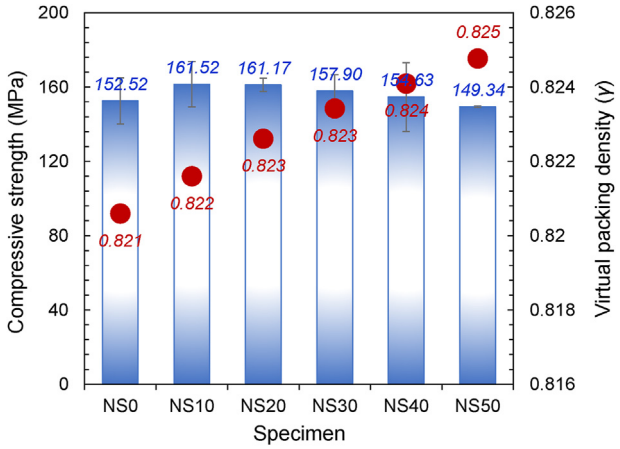

Fig. 7 – –Summary of compressive strength and virtual packing density.

setting temperature of 23 °C, the measured shrinkage strain increased and stabilized. Approximately 9 h after the casting time, the internal temperature of the specimen began to increase owing to the hydration heat, while the shrinkage strain steeply increased in the negative direction caused by the volume reduction. Owing to this initial behavior, the zeroing point must be set when measuring the autogenous shrinkage of concrete. The technical committee on autogenous shrinkage at the Japan Concrete Institute [38] recommends to measure the autogenous shrinkage after the initial setting time to exclude changes in the fresh mixture volume. Darquennes et al. [39] and ASTM C1698 [40] suggested that the initial point of autogenous shrinkage measurement of cement mortar is the final setting time. However, Yoo et al. [41] reported that if the autogenous shrinkage strain of UHPC is measured from these setting times, its shrinkage strain may be underestimated because the actual shrinkage strain occurs before the initial setting time. Therefore, in this study, the zeroing point of autogenous shrinkage was determined as the point at which the internal temperature and shrinkage strain differed.

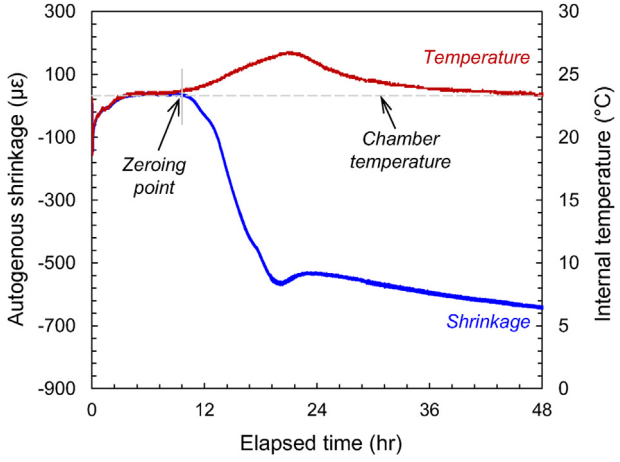

Fig. 8 – Initial strain and temperature variations of plain UHPC without nano-SiO_2.

3.4.2. *Effect of nano-SiO_2 contents on the autogenous shrinkage behavior of UHPC*

The autogenous shrinkage strain versus time curves of all specimens at an early age (up to 5 days) are shown in Fig. 9. As the content of nano-SiO_2 increases, the zeroing point of the shrinkage strain development in UHPC decreases. For example, the NS30 sample exhibited the earliest shrinkage strain development, which developed within 6.4 h after casting. This is associated with the high reactivity of nano-SiO_2. As described previously, the hydration reaction was accelerated by the considerable pozzolanic reaction of nano-SiO_2 and nucleation effect, which resulted in a steep increase in the amount of shrinkage strain at an early age. However, when the nano-SiO_2 substitution ratio exceeded 30%, the zeroing point was delayed. The NS50 sample required approximately 10.6 h to develop shrinkage strain. This is because the amount of SP used increases with an increasing nano-SiO_2 content. A delay in the hydration reaction owing to the use of SP has been reported in previous studies [42,43]. Uchikawa et al. [42] reported that the chelate complex carboxyl and hydroxyl groups of polycarboxylate molecules form a chelate complex with calcium ions (Ca^{2+}) to reduce the concentration of Ca^{2+} ions and interfere with the nucleation and hydration product growth, delaying the hydration reaction. In addition, Jansen et al. [43] explained that the withdrawal of Ca^{2+} from the pore solution by SP leads to the depletion of Ca^{2+} in the pore solution, resulting in a delay in both the silicate and aluminate reactions. Thus, the hydration reaction occurred rapidly until incorporated nano-SiO_2 reached 30%, and when the nano-SiO_2 content exceeded 30%, the hydration reaction rate gradually decreased.

Fig. 10 shows the shrinkage strain for 28 d and a comparison of the 28-day autogenous shrinkage strains. Regardless of the nano-SiO_2 content, all UHPC mixtures exhibited a significant steep increase in shrinkage strain, up to nearly 21.6 h after casting. The initial rate of increase of the shrinkage strain was significantly affected by the content of nano-SiO_2. The plain UHPC without nano-SiO_2 exhibited a relatively low

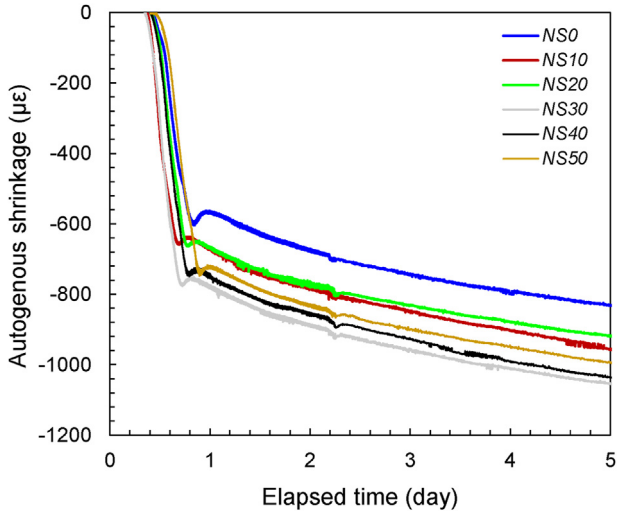

Fig. 9 – Autogenous shrinkage behavior of UHPC with various nano-SiO_2 contents up to 5 days.

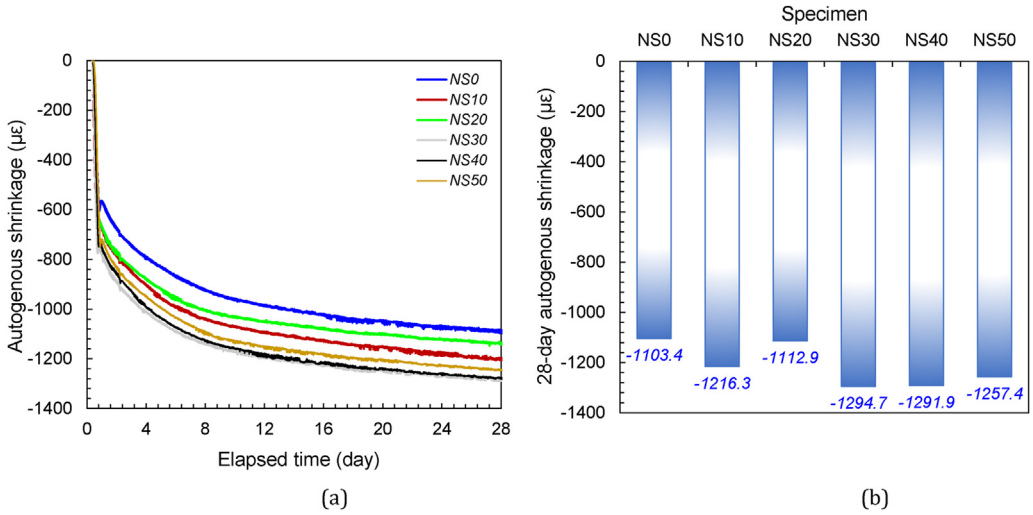

Fig. 10 – (a) Autogenous shrinkage behaviors of UHPC with various nano-SiO_2 contents: up to 28 days and (b) summary of 28-day autogenous shrinkage strains.

shrinkage increase rate at early ages, whereas the shrinkage increase rate of UHPC increased with the addition of nano-SiO_2. However, when the nano-SiO_2 content exceeded 30%, the shrinkage increase rate slightly decreased owing to the increased amount of SP and agglomeration. Therefore, the rate of increase in the shrinkage of UHPC is influenced by the content of nano-SiO_2. Similar trends were observed for the 28-day autogenous shrinkage strains in Fig. 9(b). The NS0 sample had the lowest autogenous shrinkage strain of approximately −1103 με, whereas the highest autogenous strain was found in the NS30 sample, which was approximately 1295 με, and thus 17.6% higher than that of the NS0 specimen.

To support this explanation, porosity distribution analyses of NS0 and NS30 samples were conducted using mercury intrusion porosimetry. According to the International Union of Pure and Applied Chemistry (IUPAC) [44], pores can be classified into three categories: micropores (<2 nm), mesopores (2–50 nm), and macropores (>50 nm). Moreover, Mindess et al. [45] divided pores into two categories: gel pores (<10 nm) and capillary pores (10–10,000 nm). Pores can be divided more specifically. For example, gel pores divided the pores of interlayer spaces (≤0.5 nm), micropores (0.5–2.5 nm), and small mesopores (2.5–10 nm); and capillary pores divided the large mesopores (10–50 nm) and macropores (50–10,000 nm). Here, gel pores are related to the inherent part of C–S–H gels, and capillary pores are related to the spaces between partially hydrated cementitious particles [45]. Moreover, Aligizaki [46] reported that entrained air voids (<1000 μm) and capillary pores affected the mechanical properties of hardened cement pastes. However, the very fine pores, which have diameters below 50 nm, affect the self-desiccation of the cementitious matrix.

Fig. 11 shows the pore size distribution of nano-SiO_2 incorporated UHPC mortar. The porosity distribution was divided into four parts according to the pore size: gel pores, large mesopores, macropores, and entrained air voids, as shown in Fig. 12. Although the total porosity of the NS0 sample was 4.02%, it was significantly low compared to the other types of concrete because of the highly densified microstructures of UHPC. The total porosity of the UHPC samples with a nano-SiO_2 content of 30% was lower than that of the plain UHPC without it. This decrease in porosity is attributed to the

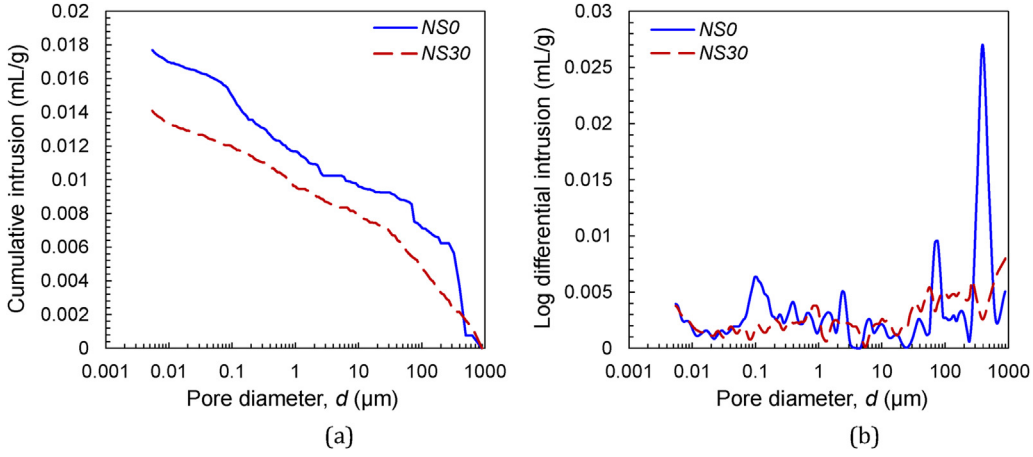

Fig. 11 – Pore size distribution of NS0 and NS30 samples: (a) cumulative intrusion and (b) log differential intrusion.

decrease in the entrained air voids and macropores, which affects the mechanical strength. However, the capillary pores containing gel pores increased with the addition of nano-SiO_2, because more abundant C–S–H gels were produced owing to the pozzolanic reaction of nano-SiO_2 and portlandite between water-filled pores and cementitious grains [30]. Therefore, the capillary pores were refined, resulting in an increase in the autogenous shrinkage, which is consistent with the findings of Meng and Khayat [34]. They noted that the refinement of pore size and increased volume of mesopores (2–50 nm) promoted a higher autogenous shrinkage owing to a strong self-desiccation.

3.5. *Single fiber pull-out behavior*

3.5.1. *Effect of nano-SiO_2 content on the pull-out behavior of aligned steel fiber in UHPC*

Fig. 13(a) depicts the average pull-out load versus slip curves. The average pull-out parameters of aligned steel fibers in UHPC with and without the nano-SiO_2 matrix are summarized in Fig. 14; they are calculated as follows:

$$\tau_{av} = \frac{P_{max}}{\pi d_f L_E}, \tag{7}$$

$$\sigma_{f,max} = \frac{P_{max}}{A_f}, \tag{8}$$

$$W_P = \int_{s=0}^{s=L_E} P(s)ds, \tag{9}$$

$$\tau_{eq} = \frac{2W_P}{\pi d_f L_E^2}, \tag{10}$$

where τ_{av} is the average bond strength (MPa), P_{max} is the maximum pull-out load in N, d_f is the fiber diameter (mm), $\sigma_{f,max}$ is the maximum tensile stress in the fiber (MPa), A_f is the cross-sectional area of the fiber (mm^2), L_E is the initial embedded length of the fiber (mm), W_p is the fiber pull-out energy (mJ), s is the slip (mm), $P(s)$ is the pull-out load in N corresponding to the slip, and τ_{eq} is the equivalent bond strength (MPa).

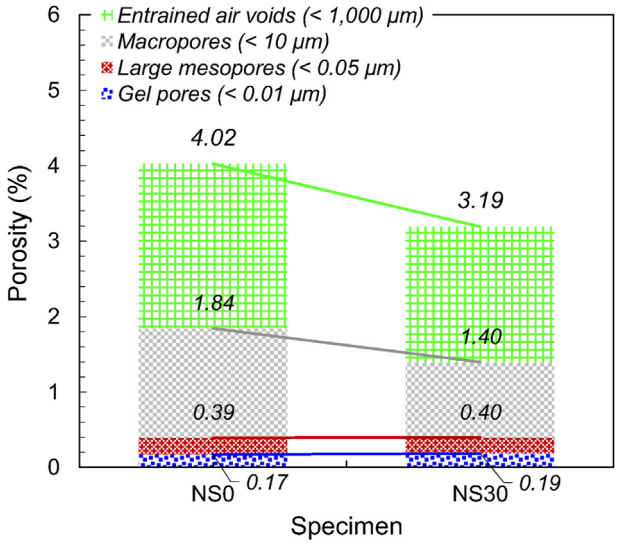

Fig. 12 – Pore volume distribution of NS0 and NS30 samples.

The plain specimen (NS0) exhibited an average bond strength of 7.17 MPa and pull-out energy of 214.7 mJ. By replacing silica fume by nano-SiO_2, the pull-out performance of the steel fibers from the UHPC matrix was improved. The best pull-out performance was obtained when 20% of silica fume was replaced by nano-SiO_2. The average bond strength and pull-out energy improved by approximately 21 and 68.3%, respectively. This improvement in bond performance is because nano-SiO_2 effectively fills the interfacial transition zone (ITZ) between the fiber and UHPC matrix. Very fine particles of nano-SiO_2 not only filled the pores of ITZ but also made it denser through the pozzolanic reaction and nucleation effect, as reported by Yoo et al. [47]. In contrast, the bond performance significantly deteriorated when the content of nano-SiO_2 exceeded 30%. Their average bond strengths were in the range of 5.59–5.91 MPa and pull-out energy was in the range of 161.4–174.5 mJ. The deterioration of bond performance was primarily owing to the agglomeration of nano-SiO_2. Nanomaterials with very fine particle sizes and large specific surface areas have a large van der Waals force; thus, when a large amount of nanomaterials is incorporated, the dispersion is degraded, decreasing the mechanical performance [30,48–50]. To explain this, the shear stress response was evaluated depending on the slip, as shown in Fig. 15. The shear stress was calculated as

$$\tau(s) = \frac{P(s)}{\pi d_f (L_E - s)}, \tag{11}$$

where $\tau(s)$ is the shear stress and s is the slip.

For the NS10 and NS20 samples, the stiffness of the shear stress in the elastic region was significantly improved and increased above 8 MPa. However, for the NS30–NS50 samples with deteriorated pull-out performances, an increase in the shear stress in the initial elastic region was similar to those of the NS10 and NS20 samples; however, full debonding occurred earlier. If nano-SiO_2 particles agglomerate in ITZ, the pozzolanic reaction occurs at the surface of the agglomerated nano-SiO_2, and nonreacted nano-SiO_2 forms a weak boundary in this zone. Thus, owing to the weak boundary at the surface of the agglomerated nano-SiO_2, the steel fibers provided lower shear strengths at ITZ, deteriorating the pull-out performance. For all tested samples, after reaching a slip of approximately 5 mm, the shear stress increased owing to the slight end deformation formed during the cutting process [51].

To verify the above explanations, SEM images of the pulled-out steel fibers from the UHPC matrices are presented in Fig. 16. The NS0 fiber was detected with some scratches, whereas the NS10 and NS20 fibers exhibited not only many more scratches but also hydration products remaining on their surfaces. Because a dense ITZ was formed by the filler, nucleation effects, and pozzolanic reaction, more scratches and hydration products were observed on the surface of the pulled-out steel fibers from the UHPC matrices. However, no obvious scratches were observed on the surfaces of the NS30, NS40, and NS50 fibers because of their significantly deteriorated interfacial bond resistance.

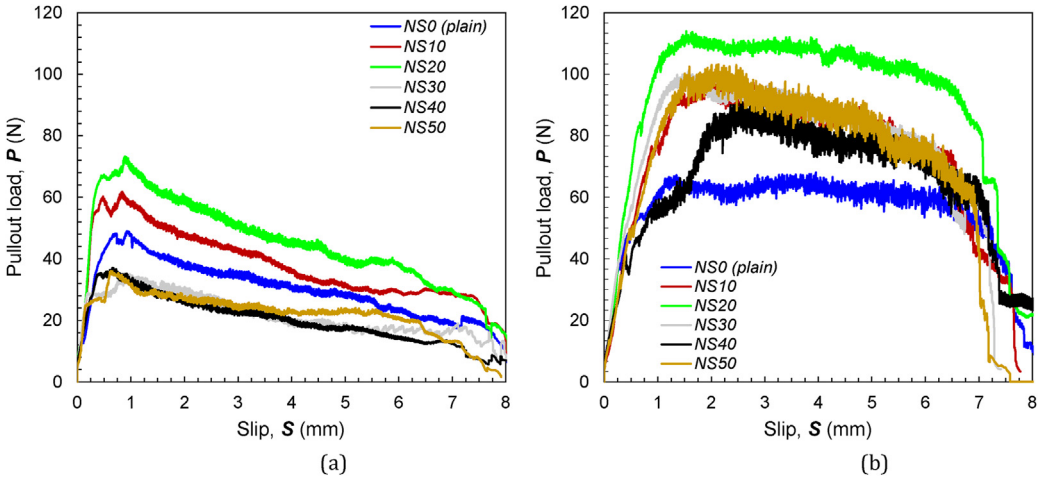

Fig. 13 – Pullout load-slip curves: (a) aligned condition and (b) inclined (45°) condition.

3.5.2. *Effect of the inclination angle and nano-SiO_2 on the pull-out behavior of steel fiber in UHPC*

Fig. 13(b) shows the average pull-out load versus slip curve of all test specimens with an inclination angle of 45°. Owing to the short embedment length of 8 mm, all test specimens exhibited a pull-out failure mode from the UHPC matrices without ruptures. The pull-out behavior was significantly affected by the fiber orientation, as reported by Lee et al. [52]. Because the fiber was inclined at 45° embedded from the UHPC matrix, the average bond strength of all test specimens

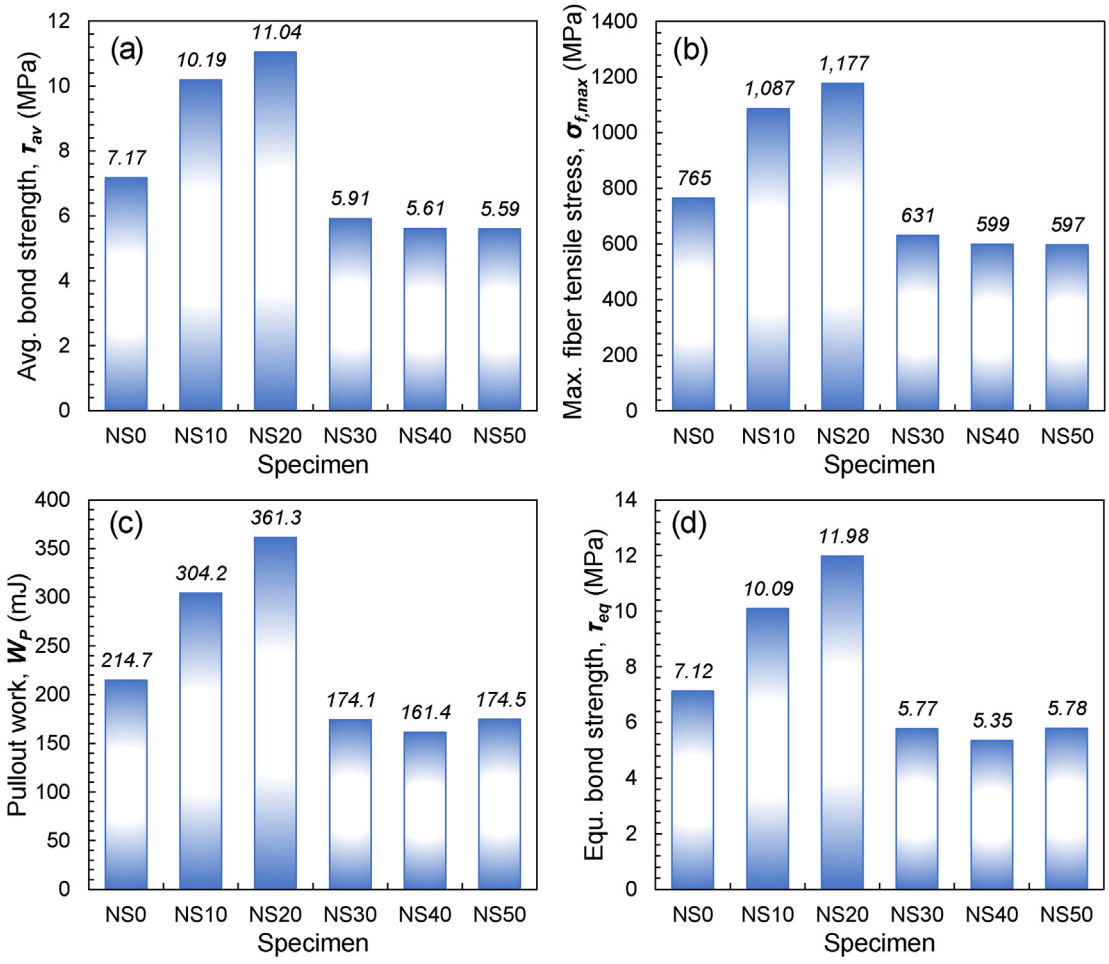

Fig. 14 – Summary of pullout parameters of aligned steel fibers in UHPC: (a) average bond strength, (b) maximum fiber tensile stress, (c) pullout work, and (d) equivalent bond strength.

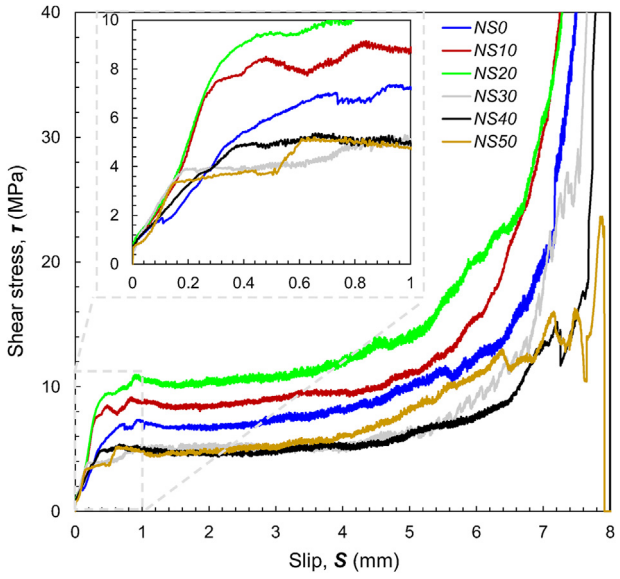

Fig. 15 – Shear stress-slip responses.

was improved by the snubbing friction effect [53]. In the aligned fiber, the slip-softening behavior was observed after reaching a maximum pull-out load owing to Poisson's effect of the fiber and abrasion of the adherent matrix particles at the interface. However, in the case of inclined steel fibers, the maximum pull-out load remained consistent with the slip, similar to the slip-hardening behavior. Pull-out parameters, such as the average bond strength, pull-out energy, equivalent bond strength, and maximum fiber tensile strength, were calculated. The pull-out performance of the aligned fibers were comparable, as shown in Fig. 17. With an increase in the nano-SiO_2 content to 20%, all pull-out parameters were improved. When the content of nano-SiO_2 exceeded 20%, however, the pull-out performance deteriorated. Thus, the highest average bond strength of 15.27 MPa was observed in the NS20 sample. However, unlike the fiber embedded in an aligned state, the pull-out performance of the NS30 and NS40 samples was higher than that of the plain NS0 sample. As for the NS50 sample, the pull-out energy and equivalent bond strength were significantly decreased to approximately 94.7% of those of the plain sample. Although nano-SiO_2 enhanced

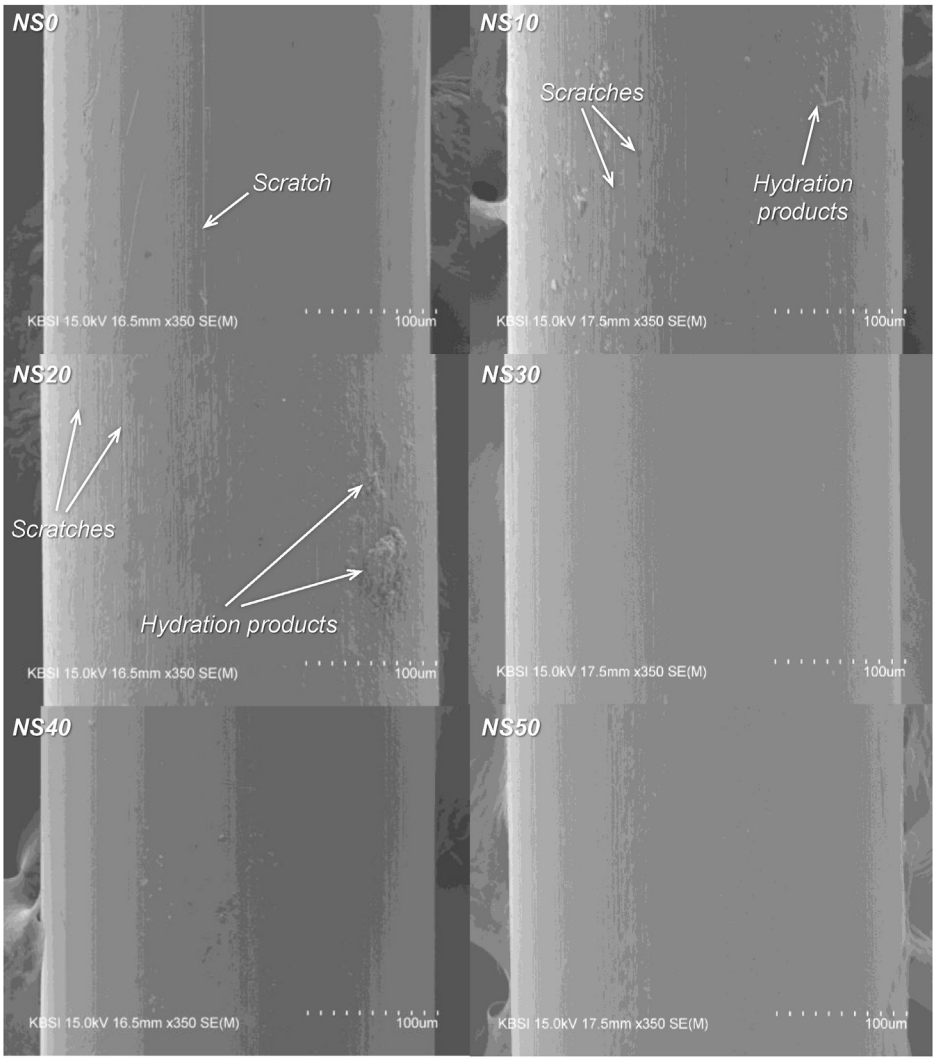

Fig. 16 – SEM image of pulled-out steel fibers from UHPC matrices.

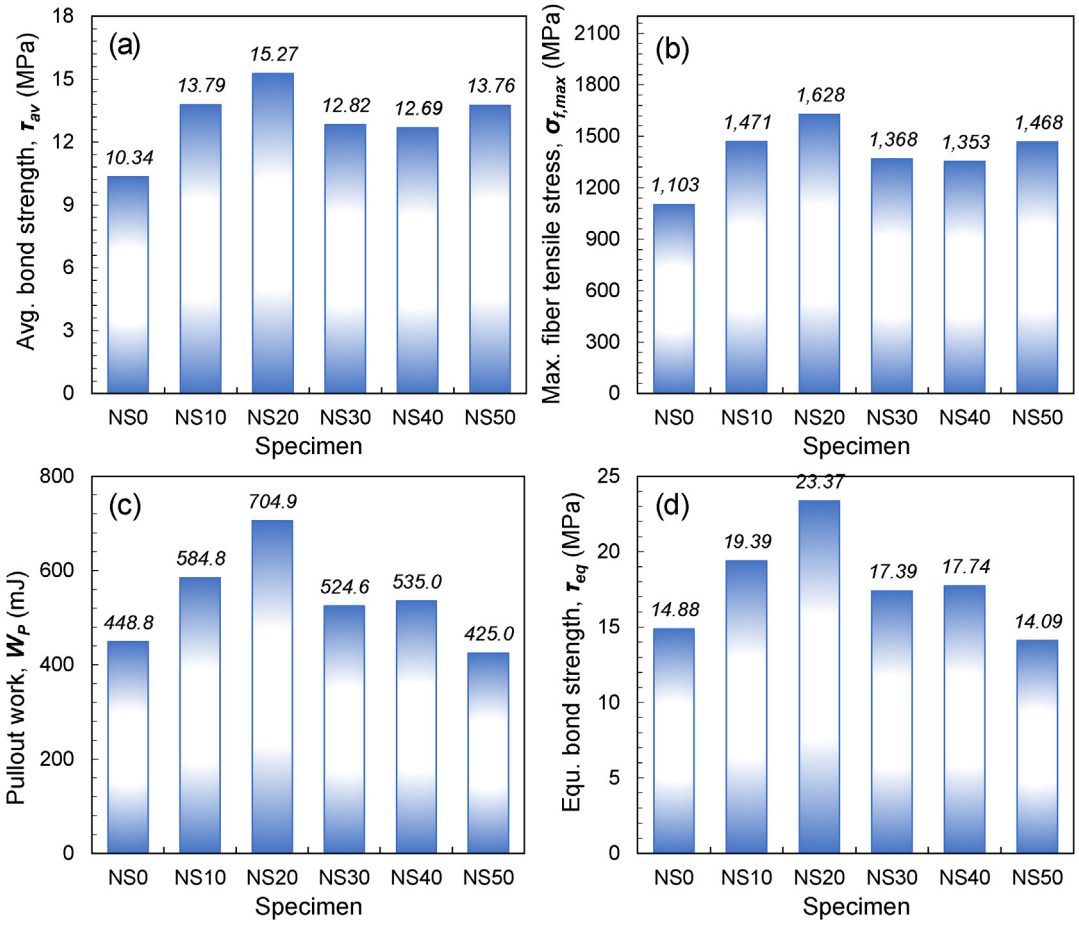

Fig. 17 – Summary of pullout parameter of inclined steel fibers in UHPC: (a) average bond strength, (b) maximum fiber tensile stress, (c) pullout work, and (d) equivalent bond strength.

the microstructures of the UHPC matrix, the agglomeration of an excessive amount of nano-SiO_2 adversely affected ITZ of the fiber and matrix, thereby decreasing the energy absorption capacity during the pull-out process.

According to Kim et al. [54], the equivalent bond strength is a good indicator to predict the tensile behavior of ultra-high-performance fiber-reinforced concrete; therefore, the increasing rate of the equivalent bond strength, according to the nano-SiO_2 content, was evaluated in Fig. 18. Regardless of the inclination angle, similar trends on the relationship between the equivalent bond strength and replacing ratio of nano-SiO_2 were found. The equivalent bond strength increasing rate increased until the amount of nano-SiO_2 to be 20%, and after that, it started to be decreased. This indicates that the optimum replacing ratio of silica fume to nano-SiO_2 is 20% by weight. The increasing rate of the equivalent bond strength of aligned steel fiber in UHPC was slightly higher than that of inclined steel fiber up to the nano-SiO_2 content of 20%, while the higher equivalent bond strength increasing rates were obtained in the inclined fiber when the content of nano-SiO_2 of 30% or higher. This might be because of the snubbing friction effect [53]. Due to the additional resistance formed at

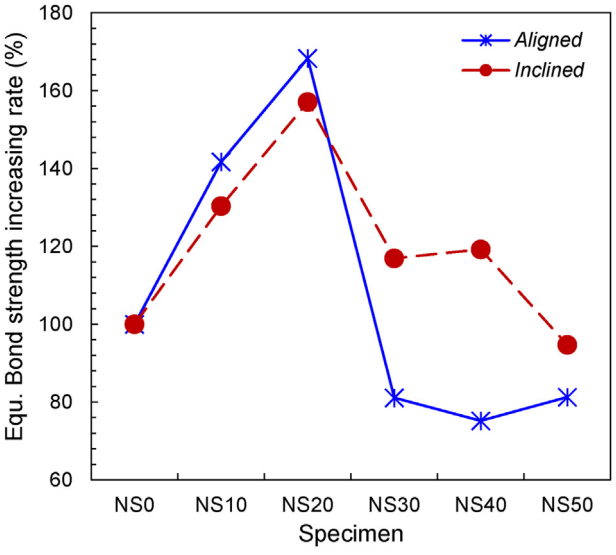

Fig. 18 – Comparative equivalent bond strength increasing rate and nano-SiO_2 content relations according to inclination angle.

the fiber exit, the decrease of fiber-matrix interfacial friction by agglomeration of nano-SiO_2 was mitigated.

4. Conclusions

This study investigated the feasibility of using large amounts of nano-SiO_2 in place of silica fume in UHPC. The degree of the pozzolanic reaction of nano-SiO_2 and its effect on the particle packing density were evaluated. In addition, the effect of nano-SiO_2 content on the compressive strength, autogenous shrinkage, and steel fiber pull-out behavior of a UHPC was analyzed. The following conclusions are drawn:

1) The nano-SiO_2 particles exhibited a remarkable pozzolanic reaction compared to other dry ingredients, such as OPC, silica fume, and silica flour. The degree of pozzolanic reaction was found to be high in the order of nano-SiO_2 >- silica fume > OPC. However, silica flour was not reactive to $Ca(OH)_2$ because of its larger grain size.
2) When a small amount of nano-SiO_2 was added, the hydration reaction was accelerated by the nucleation seed effect; however, when the content of nano-SiO_2 was more than 30%, the hydration was delayed because of the increased amount of SP and agglomeration.
3) The packing density of UHPC with nano-SiO_2 continuously increased for contents in the range of 0–50%. The trend of the compressive strength did not match that of the packing density owing to the agglomeration of nano-SiO_2 with an extremely large specific surface area. The highest compressive strength was obtained by incorporating 10% of nano-SiO_2, which was improved by 5.9% compared to that of the plain UHPC.
4) The autogenous shrinkage of UHPC increased with the nano-SiO_2 content up to 30%, similar to the initial rate of the hydration reaction; however, it became similar beyond this content. The largest autogenous shrinkage of UHPC was found to be 1295 με when nano-SiO_2 replaced 30% of silica fume.
5) The pull-out performance of steel fibers in UHPC was improved with an increase in the nano-SiO_2 content up to 20%. When 20% of the silica fume was substituted by nano-SiO_2, the average bond strength and pull-out energy improved by approximately 21 and 68%, respectively. However, when the content of nano-SiO_2 was more than 30%, agglomeration occurred at ITZ between the steel fiber and UHPC matrix, which significantly deteriorated the pull-out performance.

Declaration of Competing Interest

The authors declare that they have no known competing financial interests or personal relationships that could have appeared to influence the work reported in this paper.

Acknowledgements

This work was supported by the National Research Foundation of Korea (NRF) grant funded by the Korea government (MSIT) (No. 2021R1A2C4001503).

REFERENCES

[1] Richard P, Cheyrezy M. Composition of reactive powder concrete. Cem Concr Res 1995;25(7):1510–1.
[2] JSCE. Recommendations for design and construction of ultra-high strength fiber reinforced concrete structures (Draft). Tokyo, Japan: Japan Society of Civil Engineers (JSCE); 2004.
[3] ACI Committee 239. Ultra-high performance concrete. Toronto, Ontario: ACI Fall Convention; 2012. Canada.
[4] KCI-M-12-003. Design recommendations for ultra-high performance concrete K-UHPC. Seoul: Korea Concrete Institute (KCI); 2012.
[5] AFGC. Ultra high performance fibre-reinforced concretes. Interim recommendations. Bagneux, France: AFGC publication; 2013.
[6] Graybeal BA. Compressive behavior of ultra-high-performance fiber-reinforced concrete. ACI Mater J 2007;104(2):146–52.
[7] Ghahari SA, Ramezanianpour AM, Ramezanianpour AA, Esmaeili M. An accelerated test method of simultaneous carbonation and chloride ion ingress: durability of silica fume concrete in severe environments. Adv Mater Sci Eng 2016;2016:1650979.
[8] Yoo DY, Kang ST, Yoon YS. Effect of fiber length and placement method on flexural behavior, tension-softening curve, and fiber distribution characteristics of UHPFRC. Constr Build Mater 2014;64:67–81.
[9] Chen YW, Chu SH. Effect of silica fume on steel fiber bond characteristics in reactive powder concrete. Cem Concr res 2004;34(7):1167–72.
[10] Long G, Shi Y, Ma K, Xie Y. Reactive powder concrete reinforced by nanoparticles. Adv Cement Res 2016;28(2):99–109.
[11] Shi Y, Long G, Zen X, Xie Y, Shang T. Design of binder system of eco-efficient UHPC based on physical packing and chemical effect optimization. Constr Build Mater 2021;274:121382.
[12] Camiletti J, Soliman AM, Nehdi ML. Effect of nano-calcium carbonate on early-age properties of ultra-high-performancce concrete. Mag Concr Res 2013;65(5):297–307.
[13] Wu Z, Shi C, Khayat KH. Multi-scale investigation of microstructure, fiber pullout behavior, and mechanical properties of ultra-high performance concrete with nano-CaCO3 particles. Cem Concr Compos 2018;86:255–565.
[14] Norhasri MSM, Hamidah MS, Fadzil AM, Megawati O. Inclusion of nano metakaolin as additive in ultra high performance concrete (UHPC). Constr Build Mater 2016;127:167–75.
[15] Habeeb GM, Jeabory JM, Majeed MH. Sustainable performance of reactive powder concrete by using nano meta kaolin. J Eng Sustain Dev 2018;22(2):96–106.
[16] Shebl SS, Allie L, Morsy MS, Aglan HA. Mechanical behavior of activated nano silicate filled cement binders. J Mater Sci 2009;44:1600–6.
[17] Amin M, Abu el-hassan K. Effect of using different types of nano materials on mechanical properties of high strength concrete. Constr Build Mater 2015;80:116–24.
[18] Yu R, Spiesz P, Brouwers HJH. Effect of nano-silica on the hydration and microstructure development of Ultra-High Performance Concrete (UHPC) with a low binder amount. Constr Build Mater 2014;65:140–50.
[19] Kontolentos F, Tsakiridis PE, Marinos A, Kaloidas V, Katsioti M. Influence of colloidal nanosilica on ultrafine cement hydration: physicochemical and microstructural characterization. Constr Build Mater 2012;35:347–60.

[20] De Larrard F. Concrete mixture proportioning: a scientific approach. New York: CRC Press; 1999.
[21] Lau CK, Rowles MR, Parnham GN, Htut T, NG TS. Investigation of geopolymers containing fly ash and ground-granulated blast-furnace slag blended by amorphous ratios. Construct Build Mater 2019;222:731–7.
[22] El-Didamony H, El-Fadaly E, Amer AA, Abazeed IH. Synthesis and characterization of low cost nanosilica from sodium silicate solution and their application in ceramic engobes. Bol Soc Espanola Ceram Vidr 2020;59(1):31–43.
[23] ASTM C1856. Standard practice for fabricating and testing specimens of ultra-high performance concrete. West conshohocken, PA: ASTM International; 2017. p. 1–4.
[24] ASTM C1437. Standard test method for flow of hydraulic cement mortar. West conshohocken, PA: ASTM international; 2020. p. 1–2.
[25] ASTM C109. Standard test method for compressive strength of hydraulic cement moratrs (Using 2-in. or [50 mm] cube specimens). West conshohocken, PA: ASTM International; 2020. p. 1–12.
[26] Aïctin PC. Demystifying autogenous shrinkage. Concr Int 1999;21(11):54–6.
[27] Esteves LP. On the hydration of water-entrained cement–silica systems: comined SEM, XRD and thermal analysis in cement paste. Thermochim Acta 2011;518(1):27–35.
[28] Huang W, Kazemi-Kamya H, Sun W, Scrivener K. Effect of replacement of silica fume with calcined clay on the hydration and microstructural development of eco-UHPFRC. Mater Des 2017;121:36–46.
[29] Wang K, Shah SP, Mishulovich A. Effect of curing temperature and NaOH addition on hydration and strength development of clinker-free CKD-fly ash binder. Cem Concr Res 2004;34(2):299–309.
[30] Ghafari E, Costa H, Júlio E, Portugal A, Durães L. The effect of nanosilica addition on flowability, strength and transport properties of ultra high performance concrete. Mater Des 2014;59:1–9.
[31] You I, Zi G, Yoo DY, Lange DA. Durability of concrete containing liquid crystal display glass powder for pavement. ACI Mater J 2019;116(6):87–94.
[32] Oh T, You I, Banthia N, Yoo DY. Deposition of nanosilica particles on fiber surface for improving interfacial bond and tensile performances of ultra-high-performance fiber-reinforced concrete. Compos Part : Eng Times 2021;221:109030.
[33] Midgley HG. The determination of calcium hydroxide in set portland cements. Cem Concr Res 1979;9(1):77–82.
[34] Meng W, Khayat KH. Effect of graphite nanoplatelets and carbon nanofibers on rheology, hydration, shrinkage, mechanical properties, and microstructure of UHPC. Cem Concr Res 2018;105:64–71.
[35] Soliman NA, Tagnit-Hamou A. Using particle packing and statistical approach to optimize eco-efficient ultra-high-performance concrete. ACI Mater J 2017;114(6):847–58.
[36] Van Der Putten J, Dils J, Minne P, Boel V, De Schutter. Determination of packing profiles for the verification of the compressible packing model in case of UHPC paste. Mater Struct 2017;50:118.
[37] Ji T. Preliminary study on the water permeability and microstructure of concrete incorporating nano-SiO_2. Cem Concr Res 2005;35(10):1943–7.
[38] Japan Concrete Institute. In: Tazawa E, editor. Committee report, Autogenous shrinkage of concrete. E&FN Spon; 1999.
[39] Darquennes A, Staquet S, Espion B. Determination of time-zero and its effect on autogenous deformation evolution. Eur. J. Environ. Civ. Eng 2011;15(7):1017–29.
[40] ASTM C1698-09, Standard Test Method for Autogenous Strain of cement paste and mortar. West Conshohocken, PA: ASTM International; 2014. p. 1–8.
[41] Yoo DY, Banthia N, Yoon YS. Effectiveness of shrinkage-reducing admixture in reducing autogenous shrinkage stress of ultra-high-performance fiber reinforced concrete. Cem Concr Compos 2015;64:27–36.
[42] Uchikawa H, Sawaki D, Hanehara S. Influence of kind and added timing of organic admixture on the composition, structure and property of fresh cement paste. Cem Concr Res 1995;25(2):353–64.
[43] Jansen D, Neubauer J, Goetz-Neunhoeffer F, Haerzschel R, Hergeth WD. Change in reaction kinetics of a Portland cement caused by a superlasticizer — calculation of heat flow curves from XRD data. Cement Concr Res 2012;42:327–32.
[44] Burwel Jr RL. Manual of symbols and terminology for physicochemical quantities and units—appendix II heterogeneous catalysis. Adv Catal 1997;26:351–92.
[45] Mindess S, Young JF, Darwin D. Concrete. 2nd ed. Upper saddle River: Prentice-Hall; 2003.
[46] Aligizaki KK. Pore structure of cement-based materials: testing, interpretation and requirements. CRC Press; 2005.
[47] Yoo DY, You I. Liquid crystal display glass powder as a filler for enhancing steel fiber pullout resistance in ultra-high-performance concrete. J Build Eng 2021;33:101846.
[48] Quercia G, Hüsken G, Brouwers HJH. Water demand of amorpous nano silica and its impact on the workability of cement paste. Cem Concr Res 2012;42(2):344–57.
[49] Sobolev K, Flores I, Hermosillo R, Torres-Martínez LM. Nanomaterials and nanotechnology for high-performance cement composites. ACI Mater J 2008;254:93–120.
[50] Senff L, Hotza D, Repette WL, Ferreira VM, Labrincha JA. Influence of added nanosilica and/or silica fume on fresh and hardened properties of mortars and cement paste. Adv Appl Ceram 2009;108(7):418–28.
[51] Wille K, Naaman AE. Pullout behavior of high-strength steel fibers embedded in ultra-high-performance concrete. ACI Mater J 2012;109(4):479–87.
[52] Lee Y, Kang ST, Kim JK. Pullout behavior of inclined steel fiber in an ultra-high strength cementitious matrix. Constr Build Mater 2010;24:2030–41.
[53] Li VC, Wang Y, Backer S. Effect of inclining angle, bundling and surface treatment on synthetic fiber pull-out from a cement matrix. Compos 1990;21(2):132–40.
[54] Kim JJ, Jang YS, Yoo DY. Enhancing the tensile performance of ultra-high-performance concrete through novel curvilinear steel fibers. J Mater Res Technol 2020;9(4):7570–82.